Research Paper
J. Astron. Space Sci. 37(2), 77-84 (2020)
https://doi.org/10.5140/JASS.2020.37.2.77

JASS Journal of Astronomy and Space Sciences

Global MHD Simulation of a Prolonged Steady Weak Southward Interplanetary Magnetic Field Condition

Kyung Sun Park[1†], Dae-Young Lee[1], Khan-Hyuk Kim[2]

[1]Department of Astronomy and Space Science, Chungbuk National University, Cheongju 28644, Korea
[2]School of Space Research, Kyung Hee University, Yongin 17104, Korea

We performed high-resolution three-dimensional global magnetohydrodynamic (MHD) simulations to study the interaction between the Earth's magnetosphere and a prolonged steady southward interplanetary magnetic field (IMF) (Bz = –2nT) and slow solar wind. The simulation results show that dayside magnetic reconnection continuously occurs at the subsolar region where the magnetosheath magnetic field is antiparallel to the geomagnetic field. The plasmoid developed on closed plasma sheet field lines. We found that the vortex was generated at the magnetic equator such as (X, Y) = (7.6, 8.9) R_E due to the viscous-like interaction, which was strengthened by dayside reconnection. The magnetic field and plasma properties clearly showed quasi-periodic variations with a period of 8–10 min across the vortex. Additionally, double twin parallel vorticity in the polar region was clearly seen. The peak value of the cross-polar cap potential fluctuated between 17 and 20 kV during the tail reconnection.

Keywords: Global MHD simulation, steady state solar wind condition, quasi-periodic propagation vortex

1. INTRODUCTION

One of the significant problems in magnetospheric physics concerns the nature and properties of processes that occur at the magnetopause boundary; in particular the energy, momentum, and plasma the magnetosphere receives from solar wind. The basic processes at the magnetopause boundary are magnetic reconnection (Dungey 1961), viscous-like interaction such as the Kelvin-Helmholtz (K-H) instability (Dungey 1955; Miura 1984) and the effects of pressure pulses (Sibeck et al. 1989). In general, magnetic reconnection occurs efficiently when the interplanetary magnetic field (IMF) is southward and the rate is largest where the magnetosheath magnetic field is antiparallel to the geomagnetic field (Sonnerup 1974; Crooker 1979; Luhmann et al. 1984; Park et al. 2006). The K-H instability is driven by the velocity shear with a rapid magnetosheath plasma at the boundary, when the IMF is northward. MHD simulations showed that the K-H vortices lead to quasi-periodic variations with a period of 2.5 min for the magnetic field and plasma properties (Otto & Fairfield 2000) and vortex trains with 3–4 min periods (Ogino 2011). Guo et al. (2010) performed a global MHD simulation of the K-H instability and obtained surface waves and vortices with periods of 3–3.5 min during a northward IMF condition. The global MHD simulation by Merkin et al. (2013) showed the double-vortex sheet with vortex trains propagating along the inner and outer edges of the boundary layer. The pressure-pulse was driven by the solar wind. In particular, observations of the magnetospheric magnetic field response show quasi-periodic pulses with a period of 8 min (Sibeck et al. 1989; Sibeck 1992, 1995; Kivelson & Chen 1995). Lysak & Lee (1992) used a numerical model to show that field line resonances are dependent on the frequency of the driving pulse. Using a global MHD simulation, Claudepierre et al. (2010) found that the solar wind dynamic pressure fluctuations drive toroidal mode field line resonances on the dayside.

There have been few studies on the vortices in the magnetospheric boundary layer under southward IMF conditions. Claudepierre et al. (2008) performed high-resolution global

Received 28 APR 2020 **Revised** 28 MAY 2020 **Accepted** 1 JUN 2020
†**Corresponding Author**
Tel: +82-43-249-1750, E-mail: kspark@chungbuk.ac.kr
ORCID: https://orcid.org/0000-0002-3377-0111

MHD simulations to show that the pulsations of surface waves were generated by the K-H instability at the magnetopause boundary for varying solar wind velocities under a southward IMF condition. Our simulations are distinct from previous work by Claudepierre et al. (2008) in that the slow solar wind speed is steady in our work. Recently, statistical analysis by the Thermal Emission and Imaging Spectrometer (THEMIS) data showed that although the K-H wave rate was largest for the northward IMF, it occurred during the southward IMF. The rate was also observed to increase with solar wind speed, but was still observed at slow solar wind speeds (Kavosi & Raeder 2015).

The main purpose of this study is to investigate the role of prolonged solar wind and weak southward IMF on the magnetic configuration and vortex structure using a global MHD simulation. In Section 2, we briefly describe the simulation model, and we present the simulation results in Section 3. A summary and discussion of the results are presented in Section 4.

2. SIMULATION MODEL

We ran a three-dimensional (3D) MHD simulation with a steady and weak southward IMF and earthward solar wind flow. In this section, only a brief review of the simulation model is provided as it has been described in detail elsewhere (Ogino et al. 1992; Park et al. 2006). This model solves the normalized resistive MHD and Maxwell's equations as an initial value problem using a modified version of the Leap-Frog scheme. We used a quarter simulation box with $-90\ R_E \le X \le 30\ R_E$, $0\ R_E \le Y \le 30\ R_E$, and $0\ R_E \le Z \le 30\ R_E$ dimensions in Cartesian solar magnetospheric coordinates, assuming symmetry conditions consistent with the dipole magnetic field. The number of grid points was $(n_X, n_Y, n_Z) = (300, 100, 100)$, with a uniform grid spacing of $0.3\ R_E$. The internal ionospheric boundary conditions were set by forcing a static equilibrium at $r = 3.5\ R_E$. A mirror dipole field was applied in the solar wind at time t = 0, to take up the shape of the magnetosphere. The smoothing function dampens all perturbations near the ionosphere, including parallel currents. To obtain a quasi-steady state of the magnetospheric configuration over 4 h, we set a uniform solar wind with a number density of $n_{sw} = 5\ \mathrm{cm}^3$, a velocity of $V_{sw} = 300$ km/s and a temperature, of $T_{sw} = 2 \times 10^5$ K, with a pure southward IMF of $B_z = -2$ nT.

3. SIMULATION RESULTS

This section demonstrates the response of the magnetospheric configuration and the polar cap potential structure to steady slow solar wind and weak southward IMF condition.

The magnetic field configuration in the noon-midnight meridian plane is shown in Fig. 1. The Earth is located at the origin, closed field lines that connect to the Earth in both hemispheres are green, open field lines that connect to the ionospheres at one end and to the distant IMF at the other end are blue, and the detached field lines that do not connect to the Earth are red. The twisted pink field lines refer to the plasmoid structure in Fig. 1(b). We identify the dayside reconnection sites that lie between the regions with the highly kinked open field lines. The dayside magnetic reconnection occurs in the antiparallel field region at the dayside magnetopause as the magnetosheath flow is slower in this region. The dayside reconnection initially and continuously occurs near the subsolar region at approximately $X = 11\ R_E$. Fig. 1(a) shows the closed field line at the tail widely stretched tailward until the tail reconnection. The tail reconnection begins in the near-earth region at approximately $X = -14.4\ R_E$ from 68 min during the simulation for steady solar wind and weak IMF condition. Fig. 1(b) shows the plasmoid structure near midnight due to the tail reconnection. The tail reconnection occurs at approximately $X = -15\ R_E$ at t = 90 min. The plasmoid moves tailward with a velocity of 40 km/s up to 148 km/s when the tail reconnection continues to the lobe field lines. The tail reconnection sites move to Earth at approximately $X = -12$–$13\ R_E$ in Fig. 1(c) and 1(d).

Fig. 2 show the plasma flow vectors in the *XZ* (top) and *XY* planes (bottom) at time t = 60 min. The red lines mean the $B_Z = 0$ regions, which is the location of the magnetopause. We see in the *XY* plane view that vortices are present near the magnetopause boundary layer in the noon-dusk side. The vortex-like structures show the inner boundary magnetopause region. The vortex A region is $(X, Y) = (7.6, 8.9)\ R_E$ and the vortex B region is $(X, Y) = (3.5, 12.9)\ R_E$. The sizes of the A and B vortices are $(1.2, 2.8)\ R_E$ and $(2.5, 4.3)\ R_E$, respectively. The sense of the vortices is counterclockwise at the duskside magnetopause.

The time evolution of the plasma flow vectors in the *XY* plane (left) and the field-aligned vorticity ($\Omega_{\parallel}$) in polar region (right) is shown in Fig. 3. Here $\Omega_{\parallel} = \frac{\boldsymbol{\Omega} \cdot \boldsymbol{B}}{B}$ and $\boldsymbol{\Omega} = \nabla \times \mathbf{v}$. In the left panel, at t = 60 min, the weak earthward plasma flow appears because the tail reconnection does not begin. Vortex A is propagating tailward with a velocity of 20 km/s up to 60 km/s during simulation, while vortex B moves tailward with a velocity of 50 km/s up to 150 km/s. Otto & Fairfield (2000) performed two-dimensional (2D) MHD simulations to suggest that an average wavelength of K-H vortices is approximately $5\ R_E$ with a vortex size close to $2\ R_E$. Kivelson & Chen (1995) observed that a surface wave was propagating

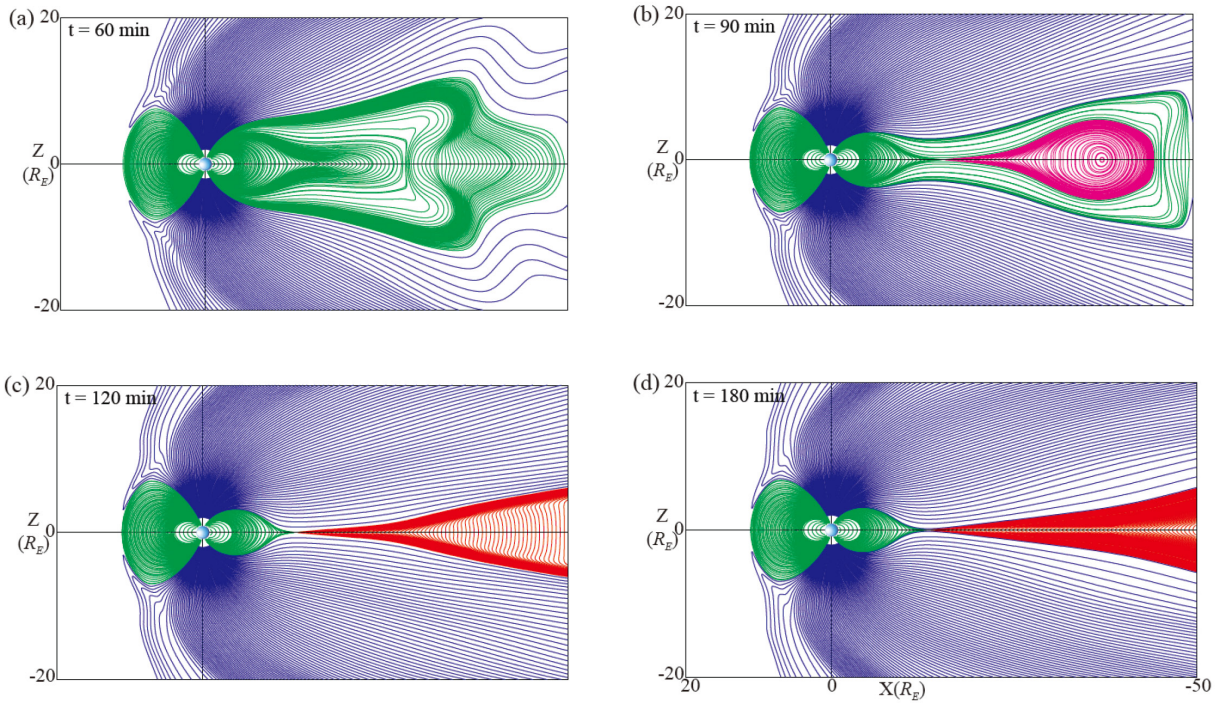

Fig. 1. Configuration of magnetic field lines in the noon-midnight meridian plane at a specific time, t = 60 (a), 90 (b), 120 (c), and 180 min (d).

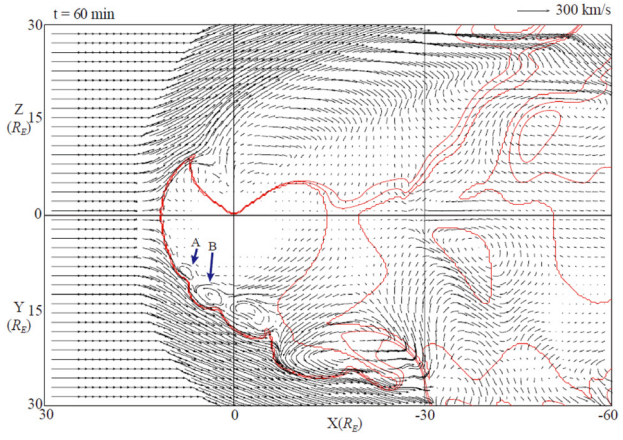

Fig. 2. The plasma flow vectors in the *XZ* (top) and *XY* planes (bottom) at time t = 60 min in simulation with IMF |**B**| = 2 nT during the weak southward IMF when the slow solar wind is in steady condition. The red lines are contours of the $B_z = 0$ region. IMF, interplanetary magnetic field.

tailward with a velocity of 90 km/s during the northward IMF. The size and propagation speed of the vortices in our simulation are similar to those obtained in these previous studies.

The bow shock was located at X =14.5 R_E and the magnetopause at X = 11 – 11.4 R_E at the nose throughout the simulation for the weak uniform southward IMF. In the right panels, the polar projections of the parallel vorticity, $\Omega_{\parallel}$, is shown in Fig. 3. The red contour corresponds to positive (parallel to the magnetic field) while the blue means negative (anti-parallel to the magnetic field). The green line represents the open-closed boundary of the magnetic field lines in the polar region. The parallel vorticity is mainly derived from the convection of closed field line through a viscous-like interaction, producing the twisting of the closed magnetic field. The vorticity was also strengthened by the dayside magnetic reconnection. In the right panel of Fig. 3, the double twin $\Omega_{\parallel}$ are clearly seen from the simulation. Viscous cell (1), the induced viscous cell (1′) and the tail lobe convection cell (2) strengthened after the tail reconnection at t = 90 min.

Fig. 4 shows the temporal fluctuations of the magnetic field and plasma properties from t = 90 min to 130 min during simulation. The data were recorded at the X = 3 R_E, Y = 12 R_E, and Z = 0 R_E location across the vortex. The center of the vortices were marked by dashed vertical lines. This figure clearly shows quasi-periodic behavior with a period of 8–10 min. The center of the vortices with a bipolar magnetic field (B_x and B_y) perturbation possesses an in-field component normal to the magnetopause with increasing total magnetic field. The velocity was low at the center of the vortices and variations in the V_x and V_y components were roughly 90 degrees out of phase. The density, plasma pressure and current were high at the center of the vortices.

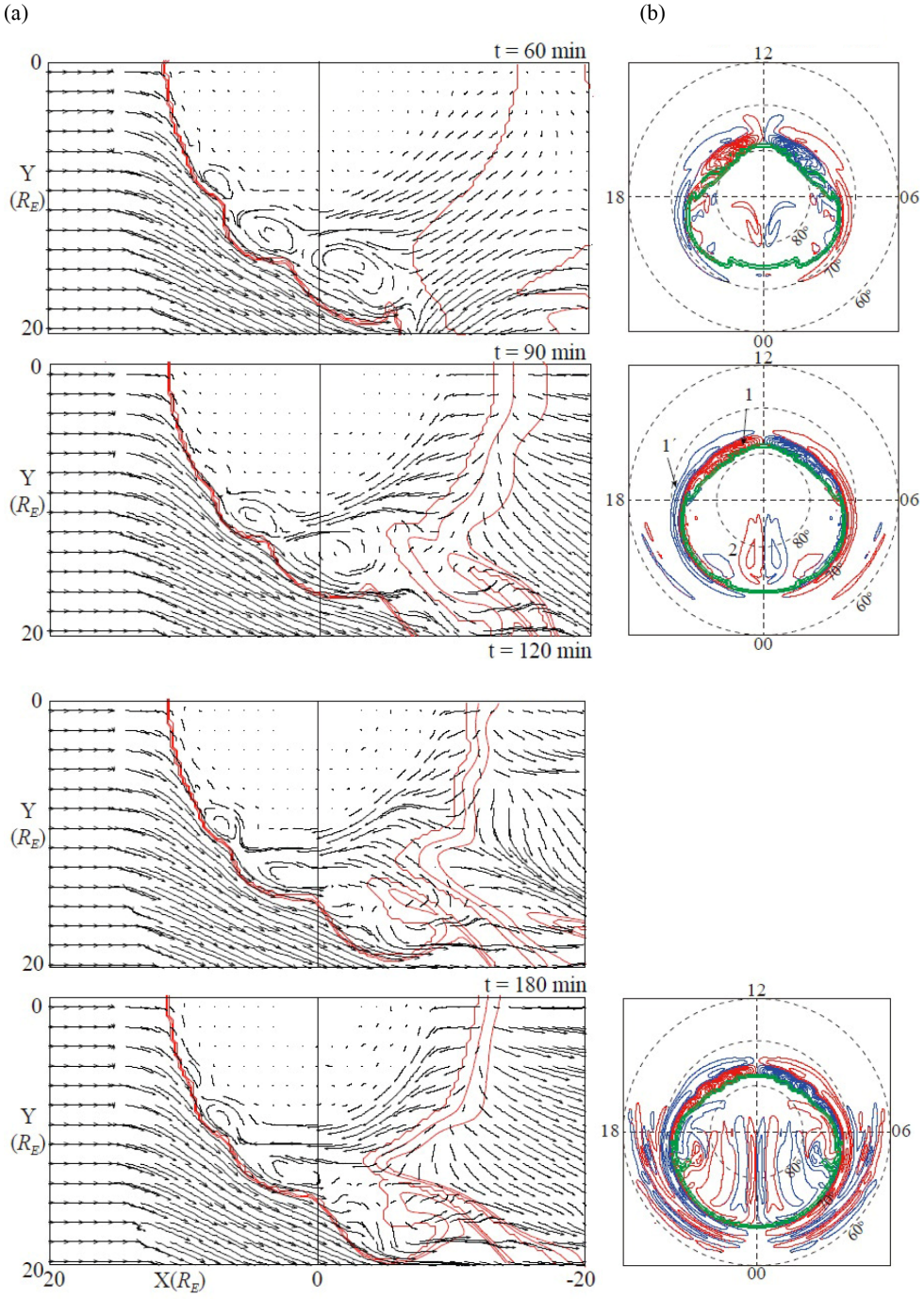

Fig. 3. The time evolution of the plasma flow (at t = 60, 90, 120, and 180 min) (a), and the parallel vorticity (at t = 60, 90, and 180 min) (b) in the polar region for the simulation.

Fig. 5(a) shows the evolution over time of the electric potential mapped onto the polar region. It reaches its maximum potential at approximately 30 kV in 16 min and then approaches steady state at approximately 20 kV. The cross polar cap potential was slightly perturbed after the tail reconnection in Fig. 5(a).

The perturbation of the cross polar cap potential also had a periodicity of 8–10 min. Fig. 5(b) shows 2D patterns of the electric potential in the polar region at selected times. The blue and red contours indicate negative and positive potentials, respectively. A double line delimits the boundary between the open and closed field lines. A two-cell pattern appears in the polar region during the simulation for weak southward IMF. At t = 60 min, the open-closed boundary

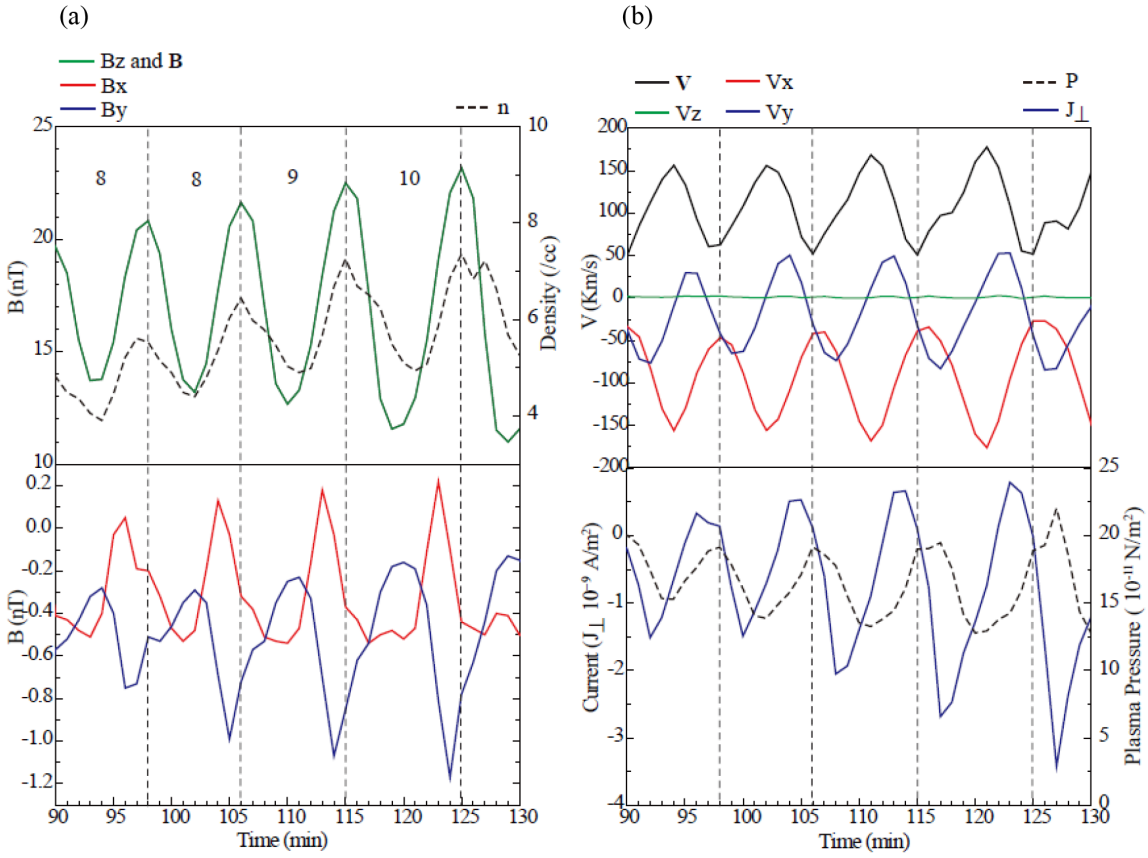

Fig. 4. The time evolution of the magnetic field and plasma density (a) and the plasma flow vector, current density and plasma pressure (b) from 90 to 130 min for the simulation. The data were recorded at the $X = 3\ R_E$, $Y = 12\ R_E$ and $Z = 0\ R_E$ location across vortex B in Fig. 2.

was 75° at night, around 80° at noon, and 75° for the dawn and dusk region. Then, the open-closed boundary extends close to 70° near midnight at t = 90 and 180 min.

4. SUMMARY AND DISCUSSION

This paper presents an investigation of the magnetospheric response using a 3D global MHD simulation when the IMF is purely weak southward and the solar wind speed is slow and steady. The main characteristics we found from this simulation were:

(i) The vortices are generated near the inner site of the magnetopause after dayside reconnection;

(ii) The vortex propagates anti-sunward with a velocity of approximately 20–60 km/s in the dayside magnetopause region and about 50–150 km/s in the duskside region of the magnetopause;

(iii) The vortex rotates counterclockwise on the duskside and clockwise on the dawnside;

(iv) Across the vortex, the magnetic field and plasma properties clearly show quasi-periodic fluctuations with a period of 8–10 min;

(v) Double twin $\Omega_{\parallel}$ are clearly visible in the polar region and the viscous cell, induced viscous cell and tail lobe convection cell strengthened after the tail reconnection; and

(vi) The peak value of the cross-polar cap potential fluctuates between 17 and 20 kV with a period of 8–10 min during tail reconnection.

We emphasize that the velocity shear exists at the dayside magnetopause boundary because the plasma flows near the magnetic equator are deformed by reconnection (Fig. 4). Thus, we suggest that reconnection plays a role in generating vortices with a periodicity in the dayside magnetopause boundary region under a weak southward IMF and steady and slow solar wind conditions.

Previous reports show the perturbations of the plasma and magnetic field in the magnetopause boundary region when the IMF was northward (Chen & Kivelson 1993; Kivelson & Chen 1995; Fairfield et al. 2000). Fairfield et al. (2000) demonstrated that the plasma quantities were highly variable with a periodicity of 3 min in the boundary region,

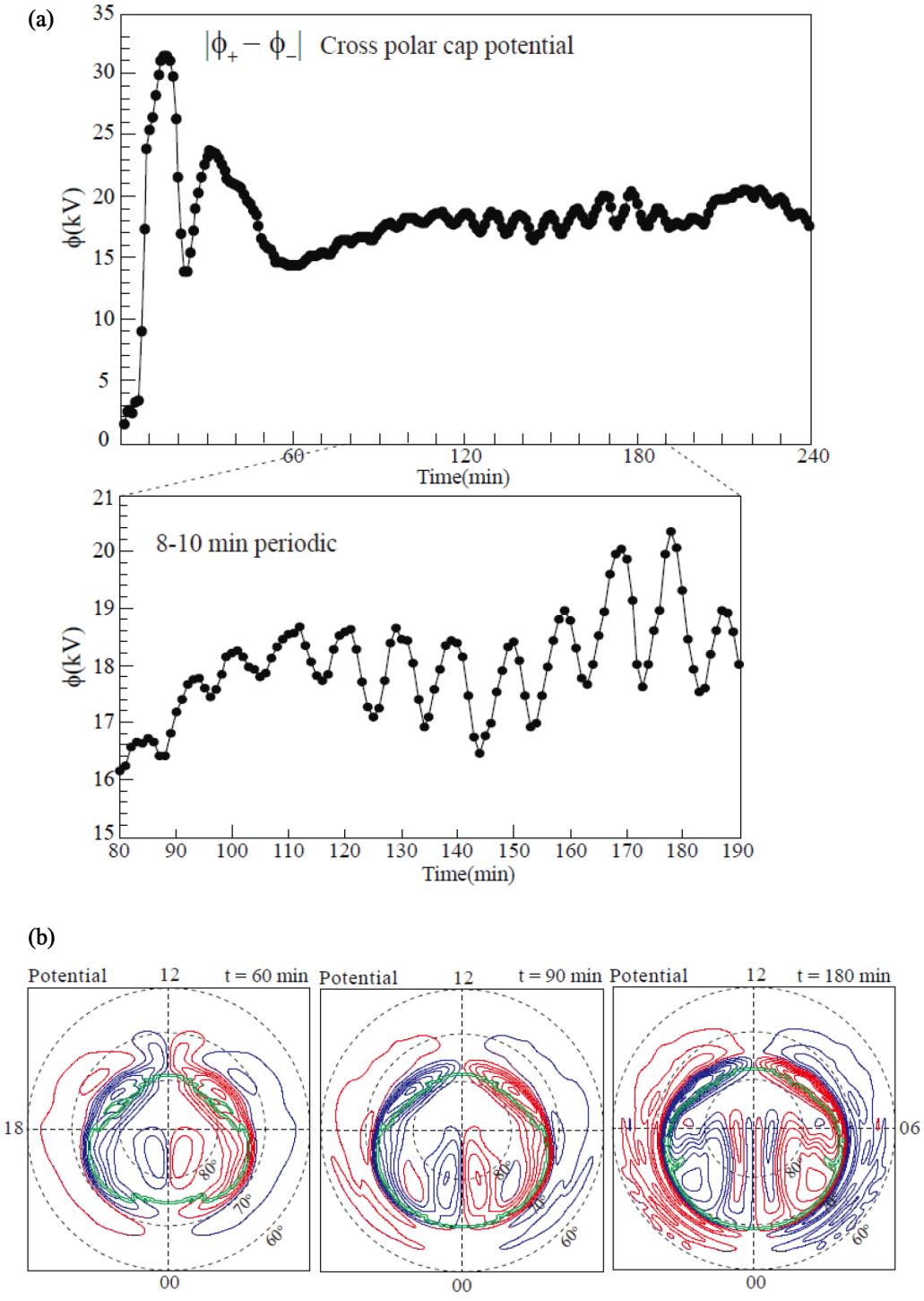

Fig. 5. The time evolution of the cross-polar cap potential (a) and the potential pattern at t = 60, 90, and 180 min (b) in the polar region.

based on Geotail observations. They showed that at the center of the vortex region, the plasma is dense and cool, and the total magnetic field increases with different polarities between B_x and B_y. These features were also appeared in our simulation results. Kivelson & Chen (1995) found wave-like fluctuations in the magnetopause where the plasma density and flow velocity were larger than those in the magnetosphere, but smaller than the magnetosheath. The vortices in our simulation show that the plasma density (approximately 1–2 cm^{-3}) and velocity (~20 km/s), increase slightly at the

inner boundary of the magnetopause. Chen & Kivelson (1993) reported that the non-sinusoidal wave steepened at the sunward facing surface at the magnetopause boundary of the tail for the northward IMF condition. Fig. 6 shows the shape of the magnetopause for (a) Chen & Kivelson (1993) and (b) our simulation results. The wave has steepened slopes anti-sunward for the 2D MHD simulation and at the sunward edge for observations in Fig. 6(a). Our 3D simulation results even under a weak southward IMF is consistent for observations in Fig. 6(b).

To the authors' knowledge, there are only a few studies on the vortex under southward IMF conditions. For the southward condition (IMF B_z = –5 nT), Walker et al. (1993) showed similar vortex structures at the dayside magnetopause. The vortices start approximately in the 15LT or 16LT region for the global MHD simulation. They suggested that the vortices may be related to the counter-streaming flow at the magnetopause caused by tail reconnection. Although not shown in this paper, we see from our simulation that at time t = 68 min, tail reconnection begins in the near-Earth region at approximately X = –14.4 R_E. The plasmoid moves tailward with a velocity of 40 km/s up to 148 km/s when tail reconnection continues to the lobe field lines. Then, the magnetic field lines of the plasmoid were disconnected from the Earth and attached to the IMF during the simulation. The occurrence of this tail reconnection was greatly delayed from vortex generation in these simulation conditions. In addition, the earthward flow was not strong in the tail region for the weak southward IMF. The maximum earthward flow was 41 km/s at time t = 68 min, and this increased to approximately 148 km/s at time t = 92 min. The earthward flow gradually decreased from time t = 93 min. Therefore, we conclude that the generation of vortex at the dayside magnetopause boundary in our simulation was not directly related to the earthward flow by tail reconnection.

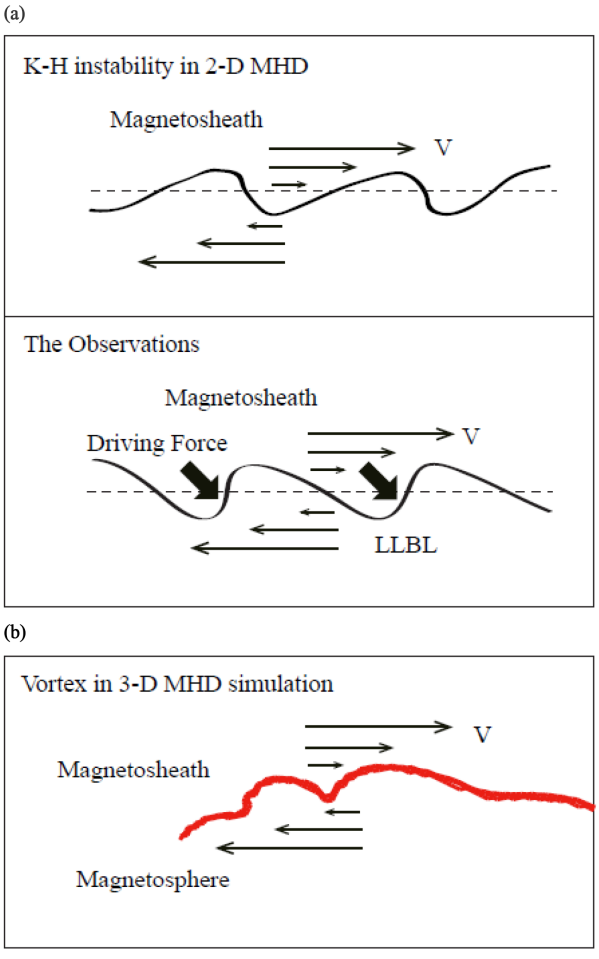

Fig. 6. A diagram for a comparison of the slope shape of the magnetopause boundary for Chen & Kivelson (a) and for our simulation results (b). Adopted from Chen & Kivelson (1993) with AGU permission policy.

Several observations have shown that ultra low frequency (ULF) pulsations are generated by solar wind dynamic pressure fluctuations in the solar wind. There are also a few simulations that have been studied for ULF waves on the dayside which may be driven by velocity shear at the magnetopause and solar wind dynamic pressure fluctuations (Claudepierre et al. 2008, 2010).

The results of this work suggest another possibility of ULF pulsations; that the periodic fluctuations of the vortex can drive ULF pulsations in the dayside magnetosphere during prolonged steady slow solar wind conditions with a weak southward IMF.

However, additional global MHD simulations are needed to clarify the effect of IMF strength, direction, and solar wind pressure on vortex generation. The simulation grid space should also be an important factor for future consideration.

ACKNOWLEDGMENTS

This research was supported by Basic Science Research Program through the National Research Foundation of Korea (NRF) funded by the Ministry of Education (No. NRF-2018R1D1A1B07043924) and by National Research Foundation of Korea (NRF) funded by Korea government (MSIP) (No. NRF-2019M1A3B2A04103464).

ORCID

Kyung Sun Park https://orcid.org/0000-0002-3377-0111
Dae-Young Lee https://orcid.org/0000-0001-9994-7277
Khan-Hyuk Kim https://orcid.org/0000-0001-8872-6065

REFERENCES

Chen SH, Kivelson MG, On nonsinusoidal waves at the Earth's magnetopause, Geophys. Res. Lett. 20, 2699-2702 (1993). https://doi.org/10.1029/93GL02622

Claudepierre SG, Elkington SR, Wiltberger M, Solar wind driving of magnetospheric ULF waves: pulsations driven by velocity shear at the magnetopause, J. Geophys. Res. 113, A05218 (2008). https://doi.org/10.1029/2007JA012890

Claudepierre SG, Hudson MK, Lotko W, Lyon JG, Denton RE, Solar wind driving of magnetospheric ULF waves: field line resonances driven by dynamic pressure fluctuations, J. Geophys. Res. 115, A11202 (2010). https://doi.org/10.1029/2010JA015399

Crooker NU, Dayside merging and cusp geometry, J. Geophys. Res. 84, 951-959 (1979). https://doi.org/10.1029/JA084iA03p00951

Dungey JW, Electrodynamics of the outer atmosphere, Proceedings of the Ionosphere Conference (The Phys. Soc. of London, 1955), 255.

Dungey JW, Interplanetary magnetic field and the auroral zones, Phys. Rev. Lett. 6, 47 (1961). https://doi.org/10.1103/PhysRevLett.6.47

Fairfield DH, Otto A, Mukai T, Kokubun S, Lepping RP, et al., Geotail observations of the Kelvin-Helmholtz instability at the equatorial magnetotail boundary for parallel northward fields, J. Geophys. Res. 104, 21159-21173 (2000). https://doi.org/10.1029/1999JA000316

Guo XC, Wang C, Hu YQ, Global MHD simulation of the Kelvin-Helmholtz instability at the magnetopause for northward interplanetary magnetic field, J. Geophys. Res. 115, A10218 (2010). https://doi.org/10.1029/2009JA0115193

Kavosi S, Raeder J, Ubiquity of Kelvin-Helmholtz waves at Earth's magnetopause, Nat. Commun. 6:7019, (2015). https://doi.org/10.1038/ncomms8019

Kivelson MG, Chen SH, The magnetopause: surface waves and instabilities and their possible dynamical consequences, in Physics of Magnetopause, eds. Song P, Sonnerup B, Thomsen M (AGU, Washington, DC, 1995), 257-268.

Lysak RL, Lee DH, Response of the dipole magnetosphere to pressure pulse, Geophys. Res. Lett. 19, 937-940 (1992). https://doi.org/10.1029/92GL00625

Luhmann JG, Walker RJ, Russell CT, Crooker NU, Spreiter JR, et al., Patterns of potential magnetic field merging sites on the dayside magnetopause, J. Geophys. Res. 89, 1739-1742 (1984). https://doi.org/10.1029/JA089iA03p01739

Merkin VG, Lyon JG, Claudepierre SG, Kelvin-Helmholtz instability of the magnetospheric boundary in a three-dimensional global MHD simulation during northward IMF conditions, J. Geophys. Res. 118, 5478-5496 (2013). https://doi.org/10.1002/jgra.50520

Miura A, Anomalous transport by magnetohydrodynamic Kelvin-Helmholtz instabilities in the solar wind-magnetosphere interaction, J. Geophys. Res. 89, 801-818 (1984). https://doi.org/10.1029/JA089iA02p00801

Ogino T, Magnetic reconnection in the magnetotail on southward turning of IMF, Proceeding of Conference on Earth-Sun System Exploration: Variability in Space Plasma Phenomena, Kona, HI, 16-21 Jan 2011.

Ogino T, Walker RJ, Ashour-Abdalla M, A global magnetohydrodynamic simulation of the magnetosheath and magnetosphere when the interplanetary magnetic field is northwards, IEEE Trans. Plasma. Sci. 20, 817-828 (1992). https://doi.org/10.1109/27.199534

Otto A, Fairfield DH, Kelvin-Helmholtz instability at the magnetotail boundary: MHD simulation and comparison with Geotail observation, J. Geophys. Res. 105, 21175-21 190 (2000). https://doi.org/10.1029/1999JA000312

Park KS, Ogino T, Walker RJ, On the importance of antiparallel reconnection when the dipole tilt and IMF B_y are nonzero, J. Geophys. Res. 111, A05202 (2006). https://doi.org/10.1029/2004JA010972

Sibeck DG, Transient events in the outer magnetosphere: boundary waves or flux transfer events? J. Geophys. Res. 97, 4009-4026 (1992). https://doi.org/10.1029/91JA03017

Sibeck DG, Baumjohann W, Elphic RC, Fairfield DH, Fennell JF, et al., The magnetospheric response to 8-minute-period strong-amplitude upstream pressure variations, J. Geophys. Res. 94, 2505-2519 (1989). https://doi.org/10.1029/JA094iA03p02505

Siscoe GL, Crooker NU, Siebert KD, Transpolar potential saturation: role of region 1 current system and solar wind ram pressure, J. Geophys. Res. 107, 1321 (2002). https://doi.org/10.1029/2001JA009176

Sonnerup BUÖ, Magnetopause reconnection rate, J. Geophys. Res. 79, 1546-1549 (1974). https://doi.org/10.1029/JA079i010p01546

Walker RJ, Ogino T, Raeder J, Ashour-Abdalla M, A global magnetohydrodynamic simulation of the magnetosphere when the interplanetary magnetic field is southward: the onset of magnetotail reconnection, J. Geophys. Res. 98, 17235-17249 (1993). https://doi.org/10.1029/93JA01321